

We are IntechOpen, the world's leading publisher of Open Access books Built by scientists, for scientists

6,900

Open access books available

186,000

International authors and editors

200M

Downloads

Our authors are among the

154

Countries delivered to

TOP 1%

most cited scientists

12.2%

Contributors from top 500 universities



WEB OF SCIENCE™

Selection of our books indexed in the Book Citation Index
in Web of Science™ Core Collection (BKCI)

Interested in publishing with us?
Contact book.department@intechopen.com

Numbers displayed above are based on latest data collected.
For more information visit www.intechopen.com



The Dynamics of Luminescence

Luyanda L. Noto, Hendrik C. Swart,
Bakang M. Mothudi, Pontsho S. Mbule and
Mokhotjwa S. Dhlamini

Additional information is available at the end of the chapter

<http://dx.doi.org/10.5772/65050>

Abstract

Domestic light providing devices have always been an important component of life and continue to provide us light beyond sunset. These devices continue to be improved frequently to allow ease of use and to enhance their efficiency. The tungsten electric light bulbs are widely used, which are based on incandescence of a continuously heated tungsten element. However, their use will soon be short lived because of the increased usage of fluorescent tubes and light-emitting diode (LED) devices, which are based on luminescence emission. These emission materials that display luminescence are called phosphors, and their emission is based on electron transitions. In the following chapter, we shall look into photoluminescence from both intrinsic and extrinsic defects, covering both down- and upconversion (UP). We will look into the concept of energy transfer and persistent luminescence and lastly provide related applications of luminescence in the modern days.

Keywords: electron traps, fluorescence, phosphorescence, kinetics, defects, persistent luminescence

1. Intrinsic and extrinsic luminescence

Luminescence occurs when a material absorbs radiation that brings about the transition of electrons from the valence band to the conduction band [1]. This is followed by de-excitation of the electrons back to the valence band via a luminescence center, which converts their energy to electromagnetic waves [2]. The luminescence center can either be from intrinsic defects [3] or from extrinsic defects [4]. **Figure 1a** shows a schematic diagram illustrating both intrinsic and

extrinsic defects. Intrinsic defects occur as a result of an atom in a matrix being displaced from its original position to an interstitial position, where it generates a point defect, leaving behind a vacancy defect [5]. Positive defects occupy the donor level (D in **Figure 1a**), and the negative defects occupy the acceptor level (A in **Figure 1a**) within the band gap of a material [6].

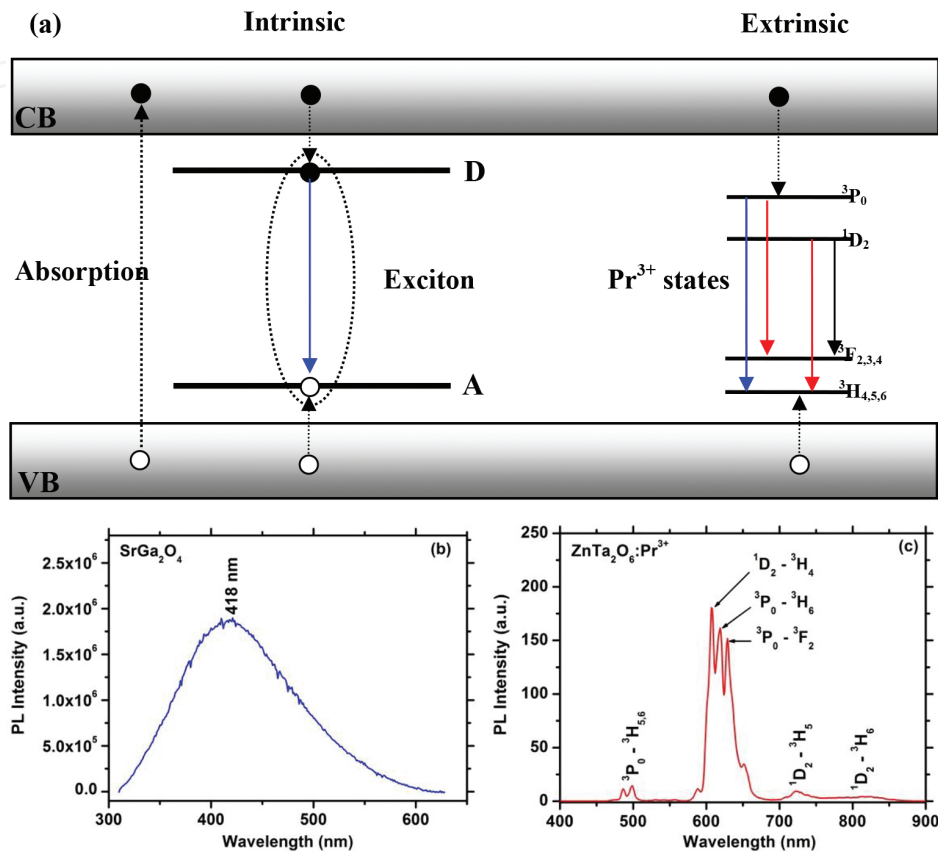


Figure 1. (a) A schematic diagram showing an emission from both intrinsic and extrinsic defects [2], (b) an emission spectrum of SrGa₂O₄ displaying luminescence from intrinsic defects, (c) shows an emission of ZnTa₂O₆:Pr³⁺ from an extrinsic luminescent center [8].

When a material with intrinsic defects absorbs radiation, the electrons are excited from the valence band to the conduction band, leaving behind positively charged holes in the valence band [4, 5]. The positive charge of the donor level exerts a coulombic force unto the excited electrons within the conduction band and attracts them. Similarly, the negative charge of the acceptor level attracts the free holes in the valence band [7]. The two will exist in a temporary bound state, and eventually the electrons will de-excite to recombine with the holes. When electrons de-excite, they lose energy, which is converted to electromagnetic waves [4, 5]. An emission spectrum showing an intrinsic defect emission of SrGa₂O₄ (unpublished data) is presented in **Figure 1b**.

Extrinsic defects are intentionally incorporated dopants into a host matrix, in order to generate a luminescent center (**Figure 1a**). When the excited electrons de-excite to the luminescent center (Pr³⁺ is used as an example of the luminescent center), further de-excite to lower state of the

center radiatively, giving electromagnetic waves with different wavelengths, depending on the ion adopted for the luminescent center [2]. It is also worth noting that direct excitation to the luminescent center occurs simultaneously with the excitation to the conduction band [5]. **Figure 1c** shows photoluminescence emission spectrum of $\text{ZnTa}_2\text{O}_6:\text{Pr}^{3+}$ phosphor, which displays blue and red emission lines from different metastates of Pr^{3+} as electrons de-excite further to their ground state. The blue emission lines are attributed to $^3\text{P}_0 \rightarrow ^3\text{H}_4$ transitions at 447–449 nm, and the red emission lines are attributed to $^1\text{D}_2 \rightarrow ^3\text{H}_4$, $^3\text{P}_0 \rightarrow ^3\text{H}_6$ and $^3\text{P}_0 \rightarrow ^3\text{F}_2$ transitions at 608, 119, and 639 nm, respectively [8].

2. Fluorescence and phosphorescence

The luminescence emission is differentiated by the length of its lifetime, which can either be fluorescent, phosphorescence, or persistent [5]. On one hand, with an emission lifetime, fluorescence is an emission lasting up to 10 ns [9]. On the other hand, phosphorescence is an emission that is longer than 10 ns, and it lasts up to 10 s [9]. Additionally, there is also an emission that lasts for a couple of minutes up to several hours after the excitation source has been removed, and it is referred to as persistent luminescence [10].

The difference between the two is explained using a simplified Jablonski diagram (**Figure 2**), which only shows transitions between vibrational states of a dopant ion. Fluorescence (F—in **Figure 2**) occurs when the energy of the incoming radiation excites an electron (A—in **Figure 2**) residing in the ground state (S_0) to higher singlet energy states ($S_1, S_2 \dots S_n$). From where the electron will de-excite to the lowest excited state (S_1), then radiatively de-excite to the ground state (S_0) within 10 ns. In the case of phosphorescence emission (P in **Figure 2**), there are triplet energy states between metastates, from which the electron stabilizes then de-excites the one below and so from T_2 to T_1 (**Figure 2**). This delayed transition of an electron results in an emission that may be delayed up to 10 s from the time of radiation absorption [11–13].

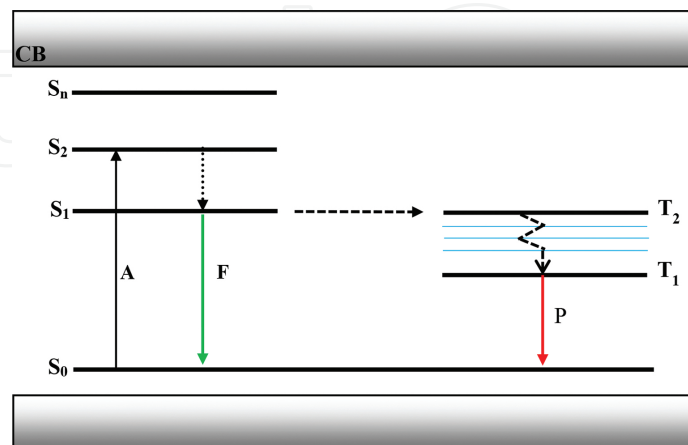


Figure 2. Schematic showing a simplified Jablonski diagram that is used to explain fluorescence and phosphorescence emission [2].

3. Persistent luminescence

Persistent luminescence differs from both fluorescence and phosphorescence, because it does not depend on the dopant ion, but the electron-trapping centers, which are generated by intrinsic defects [10]. In this case, when a sample is irradiated, the excited electrons are trapped by electron traps, and as a result of thermal energy, they gradually migrate to the luminescent center (Pr^{3+} in $\text{GdTaO}_4:\text{Pr}^{3+}$) [10, 14].

This type of luminescence may last up to several minutes or hours [10]. The decay curve (**Figure 3**) of $\text{GdTaO}_4:\text{Pr}$ shows the luminescence emission intensity change over 1200 s. It is divided into two components, the fast and the slow components, attributed to shallower and deeper electron-trapping centers [2], with time parameters that can be extracted by fitting the curve with a second-order exponential equation (Eq. (1)): where $i(t)$ is the luminescence intensity, A and B are constants, and t is the measurement time. The first and second terms describe the decay of the first and the second components; τ_1 and τ_2 represent the lifetime of the two components [15].

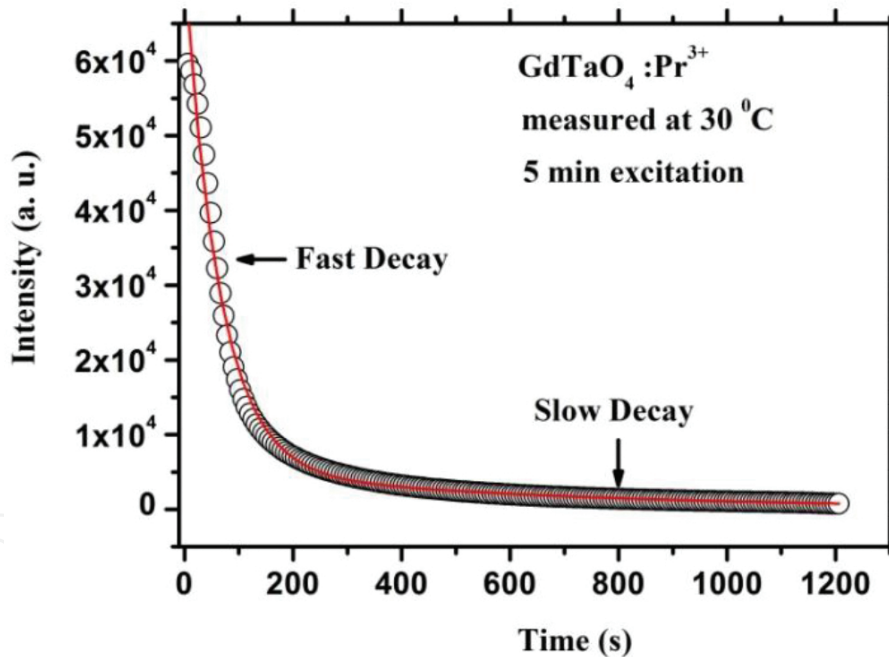


Figure 3. Decay curve of $\text{GdTaO}_4:\text{Pr}^{3+}$ persistent luminescence [2].

$$I(t) = Ae^{-t/\tau_1} + Be^{-t/\tau_2} \quad (1)$$

Persistent luminescence relies on the electron-trapping (**Figure 4**) [14] centers, which may be more than one in a particular system, and among them are positively charged oxygen vacan-

cies (V_o^\cdot and $V_o^{\cdot\cdot}$) [14–18]. These defects (oxygen vacancies) have an energy level that overlaps with energy of the conduction band, and the positively charged defects occupy the donor level, as mentioned earlier. They also occupy different energy levels relative to the conduction band [2].

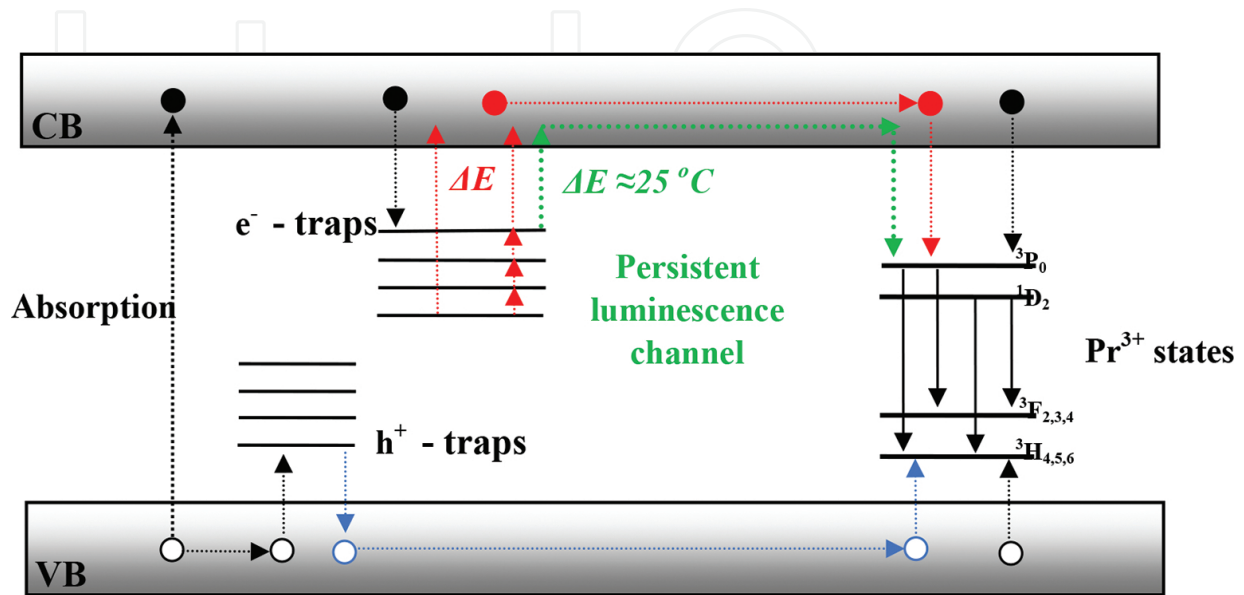


Figure 4. Schematic showing persistent luminescence mechanism for $GdTaO_4:Pr^{3+}$ [2].

The process begins by exciting the electrons to the conduction band, from where they are trapped by the electron-trapping centers [10, 14, 15], by exerting a coulombic force [7] to them. Those trapped by centers with energy levels that are equivalent to thermal energy corresponding to room temperature (shallow traps), will be detrapped and migrated to the luminescent center, via the conduction band [19]. The detrapping and migration process may last up to several minutes or hours, resulting in a phosphor displaying persistent luminescence [14–18]. The decay curve (**Figure 3**) is a measure of how the luminescence intensity resulting from the migrating electrons, changes in time. As observed, in time the luminescence intensity decreases, and this is attributed to electrons being depleted from the shallow electron traps [19].

4. Thermal-stimulated luminescence

The electrons trapped (**Figure 4**) within deeper electron-trapping centers may be thermally stimulated back to the conduction band by temperatures higher than room temperature [20]. Such luminescence is presented as a function of temperature (**Figure 5**) [21]. The resulting glow curve (**Figure 5**) is then used to approximate depth of the electron-trapping centers. Different methods may be used to calculate the depth of the electron, ranging from initial rise, Chen's peak geometry, isothermal analysis, variable heating rate, and computerized glow curve deconvolution (CGCD), among many methods [20].

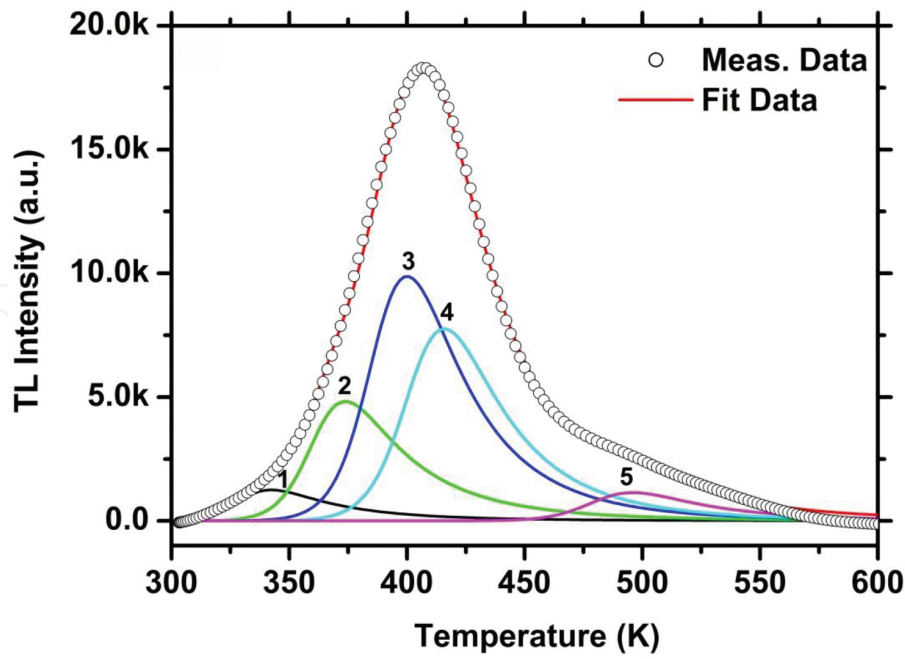


Figure 5. A deconvoluted glow-curve of $\text{ZnTa}_2\text{O}_6:\text{Pr}^{3+}$ [19].

The glow curve of $\text{ZnTa}_2\text{O}_6:\text{Pr}^{3+}$ (**Figure 5**) was deconvoluted into five thermal peaks using CGCD method, guided by the $T_m - T_{\text{stop}}$ measurements (not shown). Thermal peaks correspond to prominent electron-trapping centers with very close energy distribution within the forbidden region [22, 23]. The deconvolution was performed by the CGCD from a software package (TLAnal) developed by Chung et al. [24]. The general-order kinetics-related functions were used to compute for the activation energy (Eq. (2)), frequency factor (Eq. (3)) and the concentration of the electrons trapped within electron-trapping centers (Eq. (4)). where I_M and T_M are the TL intensity and temperature (K) at the glow peak maximum, respectively, E is the activation energy (eV), k is the Boltzmann constant, β is the heating rate, n_0 is the concentration of the trapped electrons, and b is the kinetic parameter. With the above model, the depth of the electron-trapping centers can be determined along with the quantity of electrons that were trapped [20–23].

$$I(T) = I_M b \frac{b}{b-1} \exp\left(\frac{E}{kT} \times \frac{T - T_M}{T_M}\right) \left[1 + (b-1) \frac{2kT_M}{E} + (b-1) \left(1 - \frac{2kT_M}{E}\right) \times \left(\frac{T^2}{T_M^2}\right) \exp\left(\frac{T - T_M}{T_M} \frac{E}{kT}\right)\right]^{-\frac{b}{b-1}} \quad (2)$$

$$s = \frac{\beta E}{kT_M^2 \left(1 + \frac{2kT_M(b-1)}{E}\right)} \exp\left(\frac{E}{kT_M}\right) \quad (3)$$

$$I(T) = sn_o \exp\left(-\frac{E}{kT}\right) \left[1 + \frac{s(b-1)}{\beta} \int_{T_0}^T \exp\left(-\frac{E}{kT}\right) dT\right]^{-\frac{b}{b-1}} \quad (4)$$

5. Energy transfer upconversion

In order to optimize the luminescence efficiency of a phosphor, several methods are adopted, which include energy transfer [2, 25], charge compensation [2], to mention a few. The earlier involves the energy transfer between two dopants: the activator (acceptor) and the sensitizer (donor). For the process to begin, an interaction between the two ions is required, which can either be exchange interaction, radiation reabsorption (resonant non-radiative energy transfer) or magnetic-multipole interaction [25]. There are several types of multipolar interactions involved in the energy transfer, such as dipole-dipole (d-d), dipole-quadrupole (d-q), and quadrupole-quadrupole (q-q) interactions. The process where the energy transfer occurs as radiation reabsorption is shown in **Figure 6**, where the excited donor, emits at the region where the acceptor is excited, resulting in an enhanced luminescence emission of the acceptor [26].

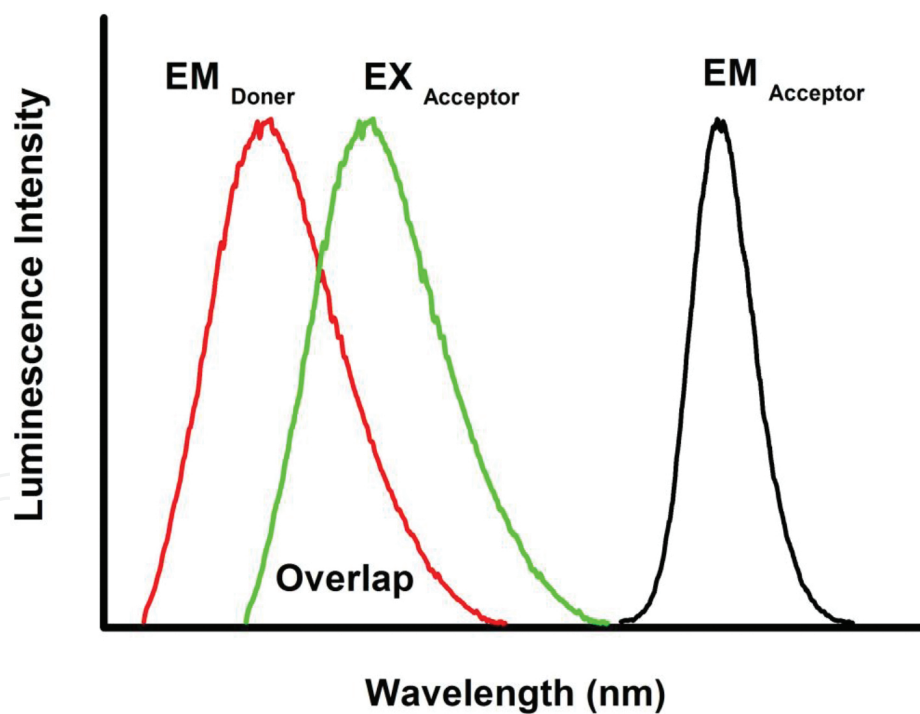


Figure 6. Schematic showing the overlap between the donor emission and the acceptor excitation.

Figure 7 shows the spectra of $\text{SiO}_2:\text{Er}^{3+}$ and $\text{SiO}_2:\text{Er}^{3+}, \text{Yb}^{3+}$. The emission of $\text{SiO}_2:\text{Er}^{3+}$ is attributed to radiative electronic transitions of Er^{3+} , which has luminescent emission peaks at 432 from ${}^4\text{F}_{5/2}$ to ${}^4\text{I}_{15/2}$, 486 from ${}^4\text{F}_{5/2}$ to ${}^4\text{I}_{15/2}$, 542 from ${}^4\text{F}_{5/2}$ to ${}^4\text{I}_{15/2}$, 611 and 708 nm from different meta-states of ${}^4\text{F}_{5/2}$ to ${}^4\text{I}_{15/2}$, as shown in **Figure 8** [27].

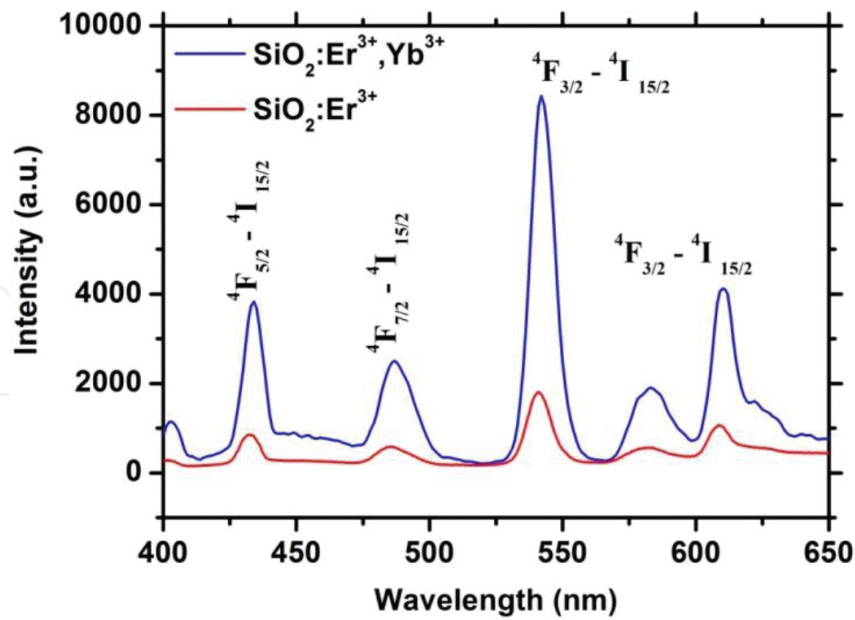


Figure 7. Luminescence from different levels of Er³⁺ energy states in SiO₂:Er³⁺ and SiO₂:Er³⁺,Yb³⁺ that were excited at 980 nm to achieve upconversion.

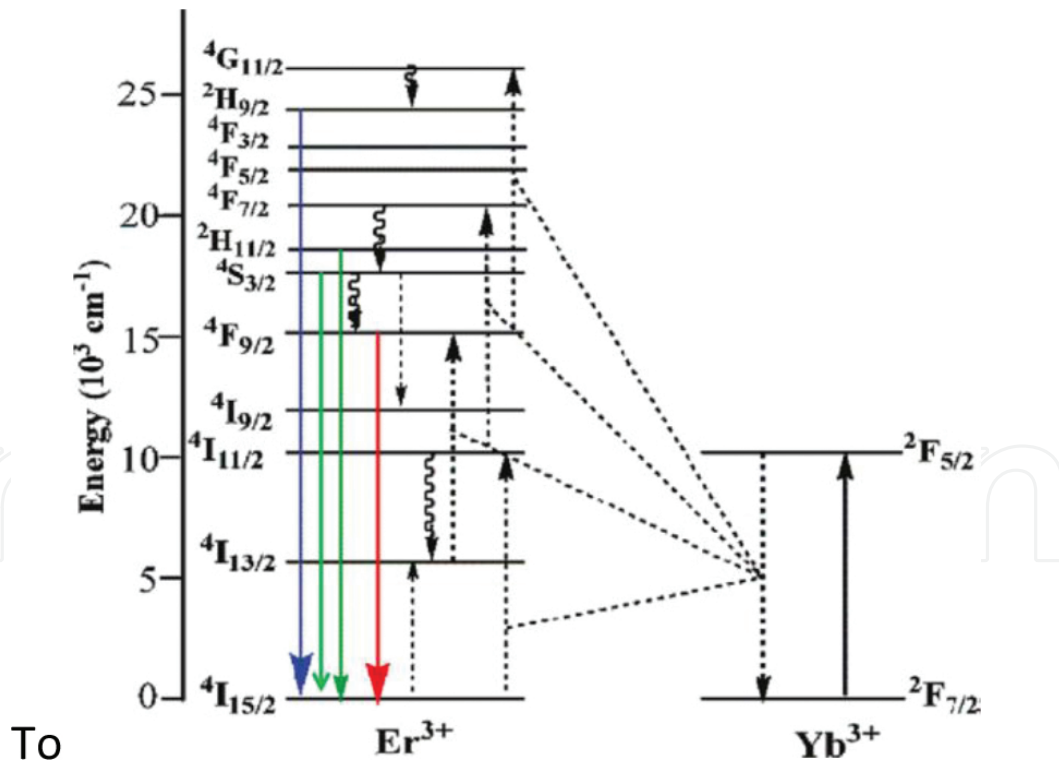


Figure 8. Jablonski energy diagram illustrating energy transfer from Er³⁺ to Yb³⁺ [28].

The luminescence of SiO₂:Er³⁺ was achieved upon exciting the sample with a 980 nm LED laser, which excited the electrons from ⁴I_{15/2} to the nearest ⁴I_{11/2} metastate or other, metastates, as

illustrated in **Figure 8**. Eventually all the small photon energies are combined to excite the electrons in a stair like process until the electrons are excited up-to the highest metastate of Er^{3+} [27]. The electrons positioned at the higher energies may de-excite directly to $^4\text{I}_{15/2}$, which is the ground state, and emit photons with energies $>$ that of the exciting source [28]. This process is referred to as upconversion (UC) luminescence [27]. Which is different from the case, where a sample is excited with high-energy photons (ultraviolet light) and yields lower-energy photons (visible, near infrared or infrared emission), as we have discussed earlier.

$\text{SiO}_2:\text{Er}^{3+}$ was co-doped with Yb^{3+} that acts as a sensitizer, in order to enhance the luminescence emission intensity of the phosphor. When the 980 nm laser is used to pump energy to $\text{SiO}_2:\text{Er}^{3+}, \text{Yb}^{3+}$, the electrons are excited from $^4\text{I}_{15/2}$ to $^4\text{I}_{11/2}$ metastates of Er^{3+} , and from $^2\text{F}_{7/2}$ to $^2\text{F}_{5/2}$ metastates of Yb^{3+} (**Figure 8**). The spectral overlap between the two ions results in the emission of Yb^{3+} that is faster than that of Er^{3+} , being absorbed, therefore transferring energy to Er^{3+} via the resonant non-radiative energy transfer channel [27]. This results in the emission of Yb^{3+} from $^2\text{F}_{5/2}$ to $^2\text{F}_{7/2}$ transition being reabsorbed to enhance the electron excitation from $^4\text{I}_{15/2}$ to $^4\text{I}_{11/2}$, $^4\text{I}_{13/2}$ to $^4\text{F}_{9/2}$ [28] and the rest of the transitions as shown in **Figure 8**.

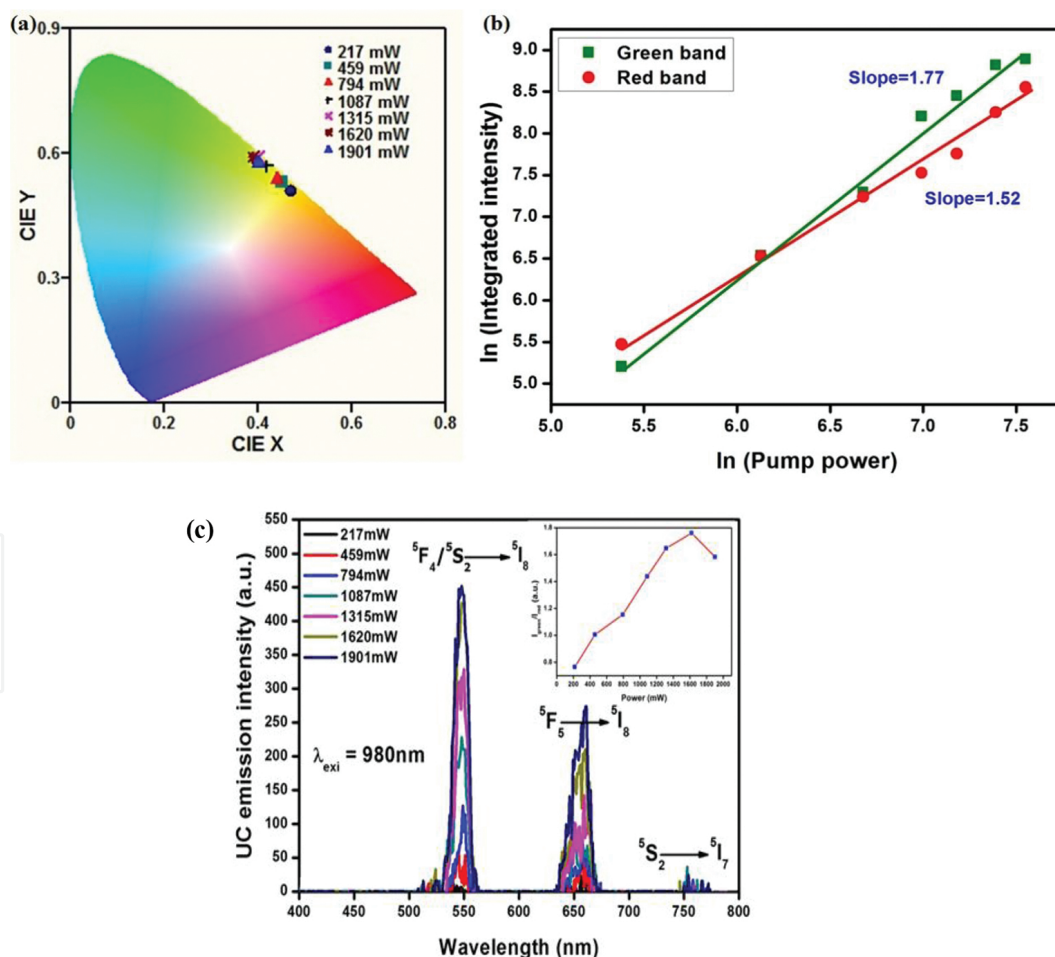


Figure 9. (a) UC emission spectra of 1 mol% Ho^{3+} -doped TZO glass on increasing excitation power (inset-green to red emission intensity ratio plot), (b) logarithmic dependence of the pump power versus integrated UC intensity, of 1 mol % Ho^{3+} -doped TZO glass, and (c) emission spectra of TZO glass doped with Ho^{3+} [30].

It is possible to determine the number of pump photons (n) involved in the UC emission process. For this, it is necessary to measure the variation of the pump power (P) as a function of the UC emission intensity (I) which is related by the following equation [29]

$$I \propto P^n \quad (5)$$

The UC emission spectra of a Ho^{3+} -doped TeO_2 -ZnO (TZO) glass recorded upon a 980 nm excitation wavelength in the 400–800 nm range at different excitation powers are shown in **Figure 9a**. Three UC emission bands were observed around 547, 660, and 760 nm in the green, red, and NIR regions, assigned to ${}^5\text{F}_4/{}^5\text{S}_2 \rightarrow {}^5\text{I}_8$, ${}^5\text{F}_5 \rightarrow {}^5\text{I}_8$, and ${}^5\text{S}_2 \rightarrow {}^5\text{I}_7$ optical transitions of Ho^{3+} ion. These transitions were aided by multiphoton excitation, and the increased intensity came about as a result of increasing the excitation power [30].

The relative intensity ratio of the green to the red emission bands changed corresponding to the excitation power as shown in the inset of **Figure 9a**. This variation in intensity was attributed to the change in their excited energy level population. **Figure 9b** shows the \ln - \ln plot of power versus UC emission intensity for the green and red emission bands of the Ho^{3+} activated TZO glass. Linear fittings of the experimental data resulted into slopes with values of 1.77 and 1.52 for the emission bands observed through the ${}^5\text{F}_4/{}^5\text{S}_2 \rightarrow {}^5\text{I}_8$ and ${}^5\text{F}_5 \rightarrow {}^5\text{I}_8$ transitions, respectively (**Figure 9c**). Thus, a two pump photon process is responsible for the UC emission from the mentioned glass system.

6. Cathodoluminescence

So far, we have mainly focused on emission that results from photon excitation and also from thermal stimulation of pre-excited electrons. In true sense, luminescence can be generated by exciting electrons via photoluminescence and cathodoluminescence and may be stimulated mechanically or thermally. Cathodoluminescence results from exciting a phosphor by an electron beam and photoluminescence by a photon beam [25]. Several properties of a phosphor may be explored by exciting it with an electron beam. However, in this chapter, we will focus on mapping as method of determining the homogeneity of the luminescence center [31], and luminescence degradation as a method of determining the chemical stability of a phosphor [2].

A commercial phosphor ($\text{CaS}:\text{Eu}^{2+}$) was exposed to the electron beam irradiation, which was accelerated using an energy of 20 keV, in 30 Pa vacuum pressure. A CL emission spectrum was obtained (**Figure 10a**), showing a broad red emission peak that is positioned at 650 nm. The peak corresponds to the radiative relaxation of the electrons from the $4f^6 5d^1 (t_{2g})$ to the $4f^7 ({}^8\text{S}_{7/2})$ of Eu^{2+} . A CL map (**Figure 10b**) was obtained by collecting several spectra from a $44 \times 32 \mu\text{m}$ field of view, at the same time as the backscattered electron (BSE) image (**Figure 11**) was obtained. The CL map comes with a scale bar indicating the intensity changes of the luminescence emission at different points along the scanned area. More luminescence intensity came from the smaller and spherical-shaped particles, than from the bigger and octahedral-shaped particles. This is an indication that the dopant (Eu^{2+}) is better incorporated in the smaller

particles and not homogeneously incorporated throughout the particles of the phosphor powder. Along with the BSE image (Figure 11), the X-ray maps (Figure 11) were obtained, confirming the presence Ca and S from CaS, and O attributed to a secondary phase (CaSO₄) [31].

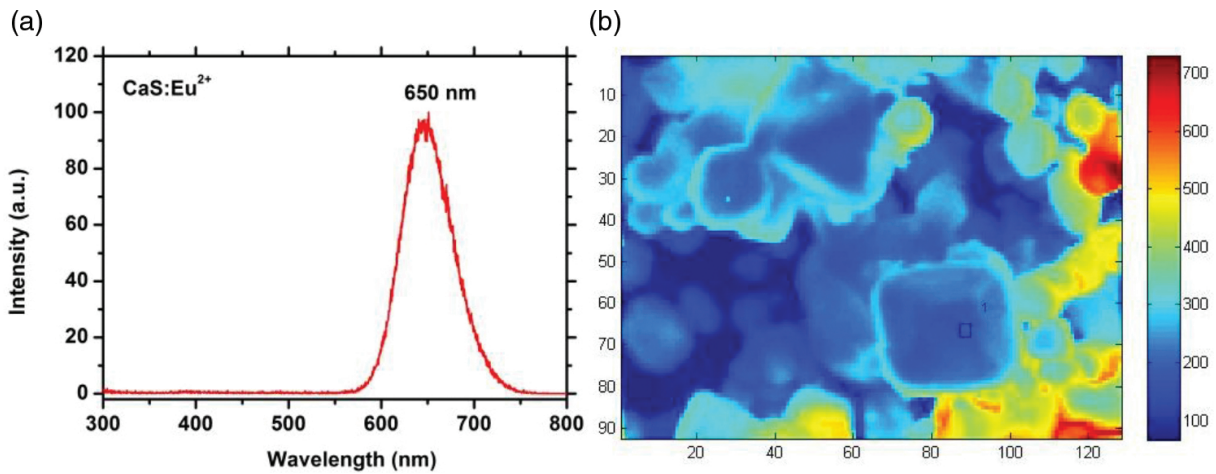


Figure 10. (a) CL spectrum and (b) map of CaS:Eu²⁺ [31].

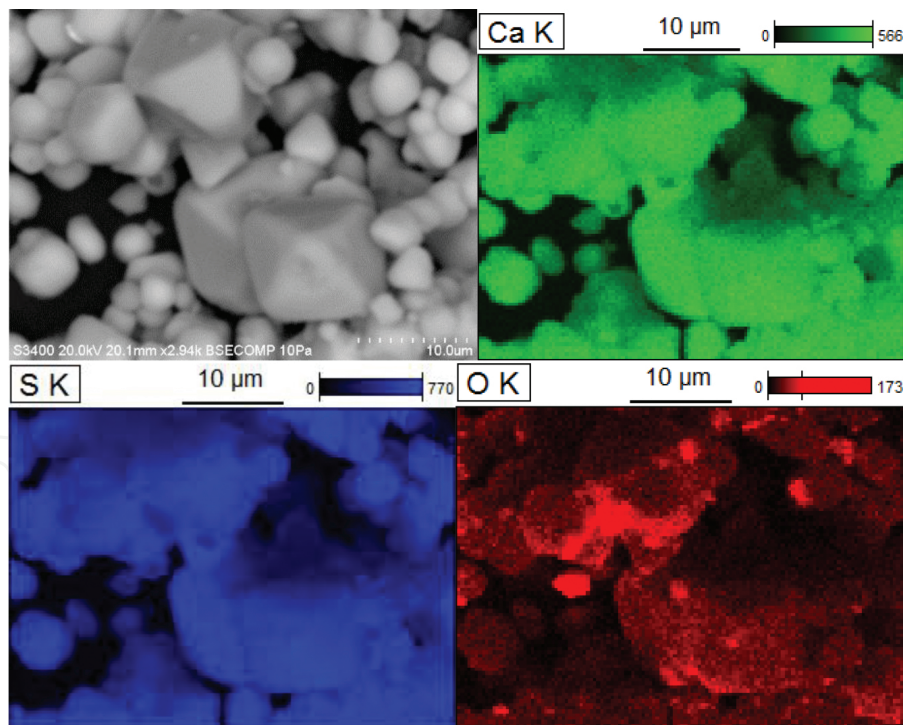


Figure 11. The BSE image and X-ray maps of CaS:Eu²⁺ commercial phosphor [31].

The surface chemical stability is an important parameter for phosphors that are projected for industrial purposes, such as manufacturing of the television and mobile phone display screens, to mention a few. The adopted laboratory procedure to investigate the chemical stability of a

particular compound is to expose its surface to harsh conditions and then monitor CL degradation. Such is achieved by accelerating a prolonged electron beam on the surface of a sample. $\text{CaTiO}_3:\text{Pr}^{3+}$ was subjected to a prolonged electron beam irradiation *in-situ*, using an Auger electron spectroscopy at 1×10^{-6} Torr O_2 , which was oxygen backfilled [2].

The resulting effects may lead to a completely degraded CL intensity, if the sample surface is not chemically stable [2]. The CL spectra of $\text{CaTiO}_3:\text{Pr}^{3+}$ (**Figure 12a**) before and after degradation are presented, which show that the luminescence intensity degraded by approximately 50%.

During the degradation process, the variation of the chemical species on the surface was monitored and plotted as the Auger peak to peak height (APPH) profile (**Figure 12b**). The introduction of O_2 in the system led to a fast oxidation of the surface of the sample, which is observed from 0 to 500 C cm^{-2} electron doses (**Figure 12b**). This is attributed to the reactive O^- species that attacked the surface of the phosphor, which was generated by the electron beam interaction with either the O_2 or H_2O or both inside the chamber, according to the ESSCR mechanism [2, 32, 33]. As a result of the electron-stimulated surface chemical reactions at the interface of the new forming surface and the real surface, a defect grows, which is responsible for the quenched luminescence intensity [2].

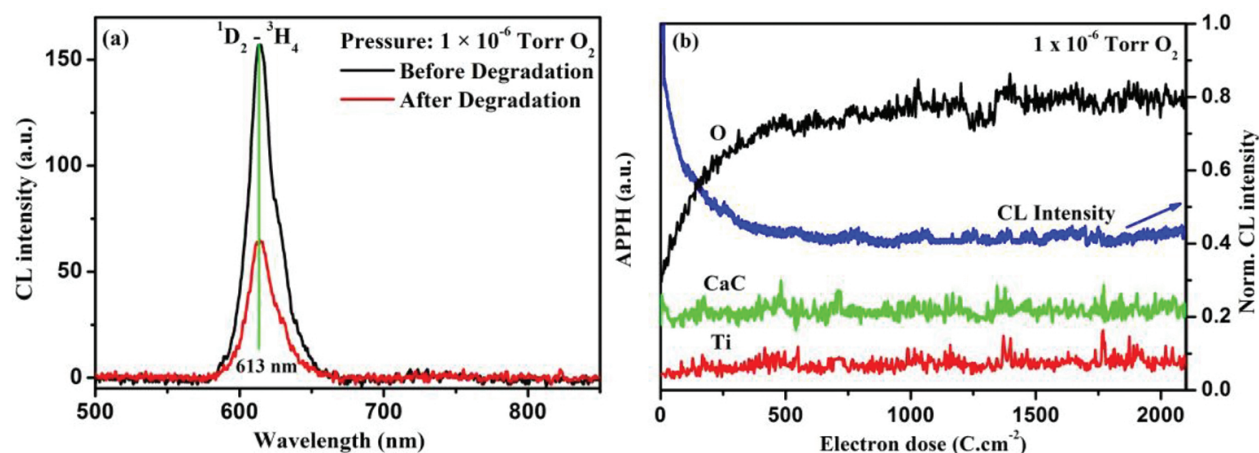


Figure 12. (a) CL spectra and (b) APPH profile of $\text{CaTiO}_3:\text{Pr}^{3+}$ irradiated with a prolonged electron beam [2].

After having probed the sample with an electron beam, X-ray photoelectron spectroscopy (XPS) was used to investigate the chemical changes that took place during the process. **Figure 13**, shows fitted XPS spectra, indicating the chemical state of the surface of the sample. The oxygen peak O 1s consists of five peaks prior degradation, contributed by peaks at 529.2 eV binding energy (BE) from the matrix (CaTiO_3), 530.4 eV BE from TiO_2 and Ti_2O_3 , 531.6 eV BE from the OH^- group bonded species. The last two peaks at 532.7 and 534.2 eV correspond to the Si-O-Si species from the silica crucible that was used to prepare the material, and from the chemisorbed species, respectively. The O 1s XPS peak of the sample that was subjected to electron beam degradation, was deconvoluted into seven peaks, with the additional peaks at

528.4 from the CaO formed on the surface as a result of surface oxidation, and at 529.8 eV BE as a result of CaO_x sub-oxide formation [2].

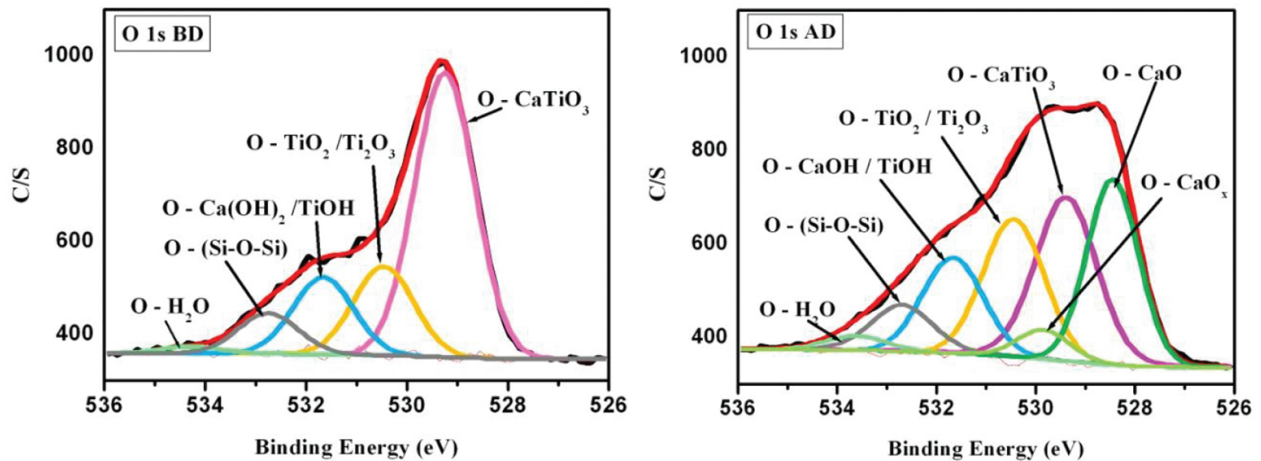


Figure 13. Spectra of O 1s before (O 1s BD) and after (O 1s AD) degradation [2].

7. Applications

There are several applications of luminescent materials; however, we will focus only on a few, which are of modern technological innovation. Such as the persistent luminescence for home lighting, luminescence for biological imaging, temperature sensing, white phosphor converted light-emitting diodes, and phosphors for a television display.

7.1. Home lighting

Persistence luminescence offers an alternative lighting that is cost-effective and energy conservative. It offers the possibility of having a light bulb that gives out light without any

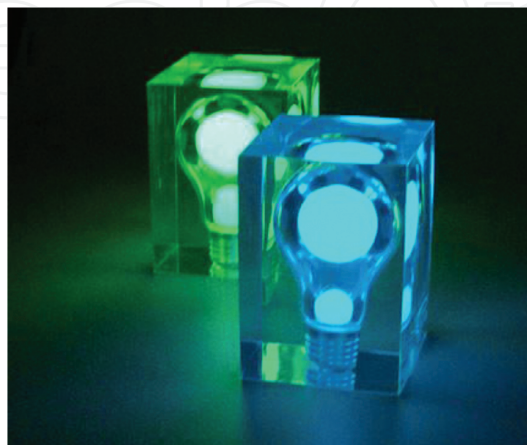


Figure 14. Light bulbs made of luminescent materials [34].

electrical connection (**Figure 14**). Such a bulb will be made of a persistent luminescent material, can be placed outside during the day to absorb the sunlight, and then placed back inside the house, where it will continue to glow in the absence of the excitation source [19].

7.2. Biological imaging

Photoluminescence mapping enables tracking of drug delivery to assess the effectiveness of the drug release. The photoluminescence functionalized drugs are employed to detect and quantify a particular disease [35, 36]. A similar approach was adopted using zinc gallate doped with chromium ions, to map the path of the luminous drugs through the gastrointestinal tract, after an oral consumption [35]. An LED was used to excite the luminous drug that was fed to a mouse (**Figure 15**) [35], which glows in the spots where the luminous drug was situated.

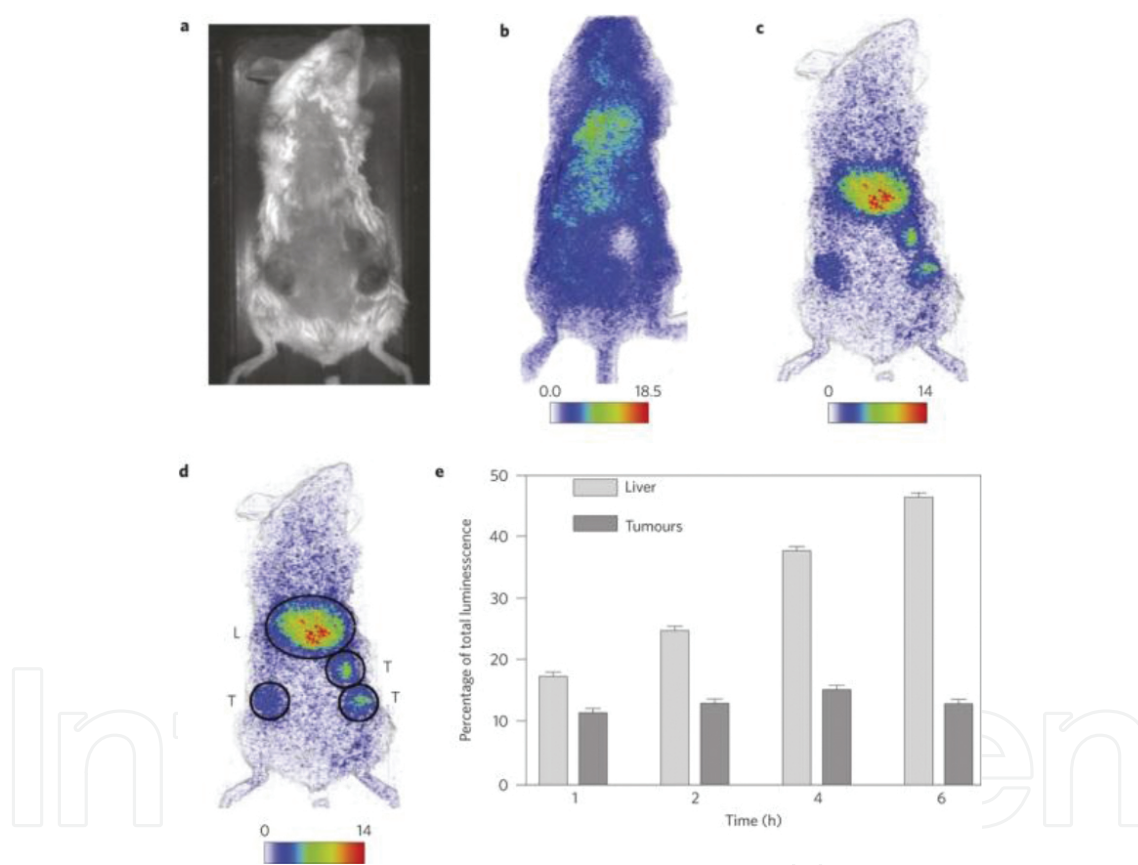


Figure 15. Schematic showing mapped luminescence of zinc gallate and poly-ethylene glycol composite [35].

7.3. Temperature sensing

Distant objects can best be measured using optical temperature sensors. Upconversion sensors modified from inorganic materials doped with rare-earth ions are proving to be better candidates in this regards [36]. Upconversion-modified sensors make use of the luminescence changes from two close metastates of a luminescence center to derive the optical temperature

changes [37]. A total of 2000 cm^{-1} is a maximum required energy difference in between these metastates, for the sensor to be effective [38]. The fluorescent intensity ratio (FIR) is then used to approximate the temperature that corresponds to the fluorescence of the thermally coupled levels [36, 39]. The fluorescence intensity ratio of thermally coupled transitions can be presented as (Eq. (6)): where I_{525} and I_{547} are the integrated intensities corresponding to the ${}^2\text{H}_{11/2} \rightarrow {}^4\text{I}_{15/2}$ and ${}^4\text{S}_{3/2} \rightarrow {}^4\text{I}_{15/2}$ transitions, respectively, B is the pre-exponential constant, ΔE is the energy difference between the ${}^2\text{H}_{11/2}$ and ${}^4\text{S}_{3/2}$ levels, k is Boltzmann's constant, and T is absolute temperature [40, 41].

$$FIR = \frac{I_{525}}{I_{547}} = B \exp\left(\frac{-\Delta E}{kT}\right) \quad (6)$$

The optical temperature sensing behavior of $\text{Er}^{3+}\text{-Yb}^{3+}$ co-doped SrWO_4 phosphor upon 980 nm excitation in the 510–570 nm range on increasing the temperature up-to 518 K have been recorded keeping the power constant as shown in **Figure 16** [42]. The integrated intensity of the UC emission bands around 525 and 547 nm (assigned through the ${}^2\text{H}_{11/2} \rightarrow {}^4\text{I}_{15/2}$ and ${}^4\text{S}_{3/2} \rightarrow {}^4\text{I}_{15/2}$ transitions of the Er^{3+} ion, respectively) varied when increasing the temperature of the sample. At room temperature (300 K), the intensity of both the transitions was nearly equal, whereas at 518 K, the intensity corresponding to the ${}^4\text{S}_{3/2} \rightarrow {}^4\text{I}_{15/2}$ transition was more reduced than that of the ${}^2\text{H}_{11/2} \rightarrow {}^4\text{I}_{15/2}$ transition. The observed change of the two transitions is plotted as the intensity ratio ($I_{525\text{nm}}/I_{547\text{nm}}$), which is a function of temperature (inset of **Figure 16**) [31].

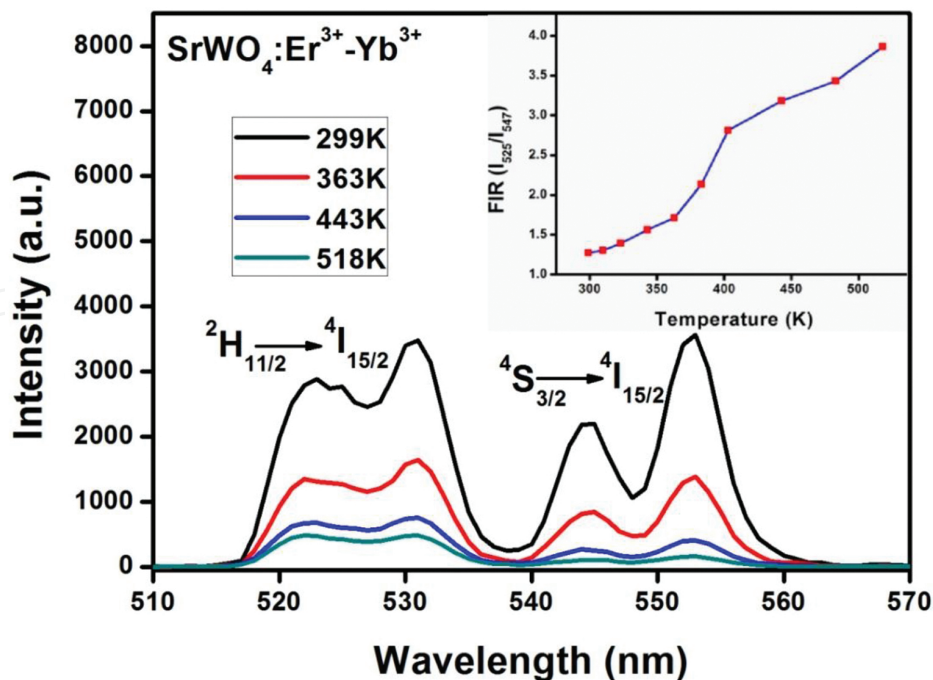


Figure 16. Green UC emission spectra of $\text{SrWO}_4:\text{Er}^{3+}\text{-Yb}^{3+}$ phosphor on increasing temperatures and the variation of FIR as function of absolute temperature (inset) [42].

In accordance with Eq. (6), the $\ln(I_{525}/I_{547})$ is plotted against the inverse absolute temperature as shown in **Figure 17**. The experimental data were linearly fitted and gave a slope equal to 866. This resulted into the energy difference value ΔE of the two thermally coupled levels of about 600 cm^{-1} .

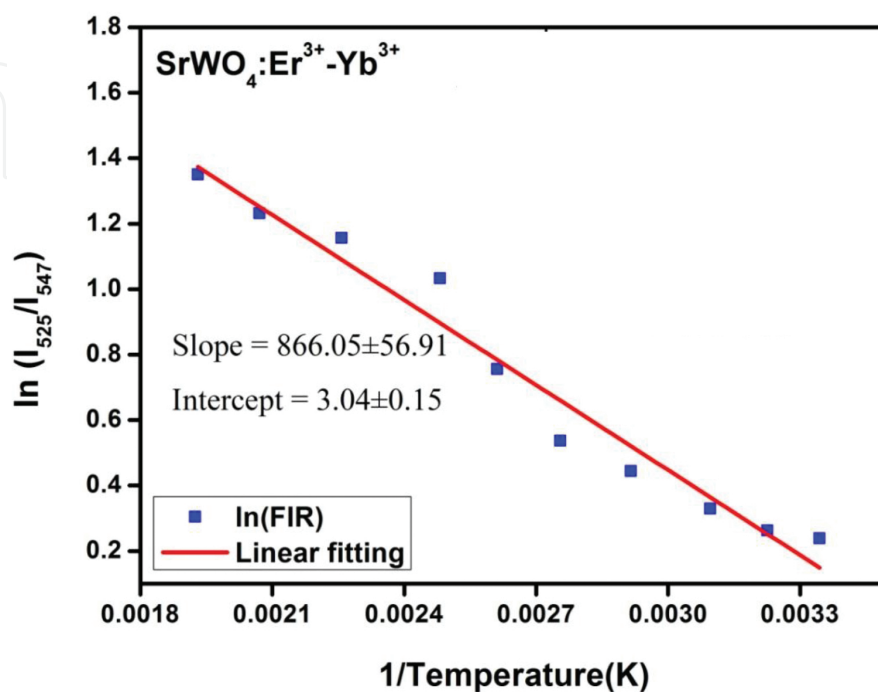


Figure 17. Plot of logarithmic of FIR versus the inverse absolute temperature [42].

7.4. Wp-LEDs

LEDs are a form of solid-state lighting technology that relies on the inorganic compounds to convert electricity to light. Recently, a blue-emitting light diode was achieved using InGaN by a team of scientists led by Isamu Akasaki, Hiroshi Amano and Shuji Nakamura [37]. An LED displaying an efficiently white emission compared to the conventional incandescent lighting

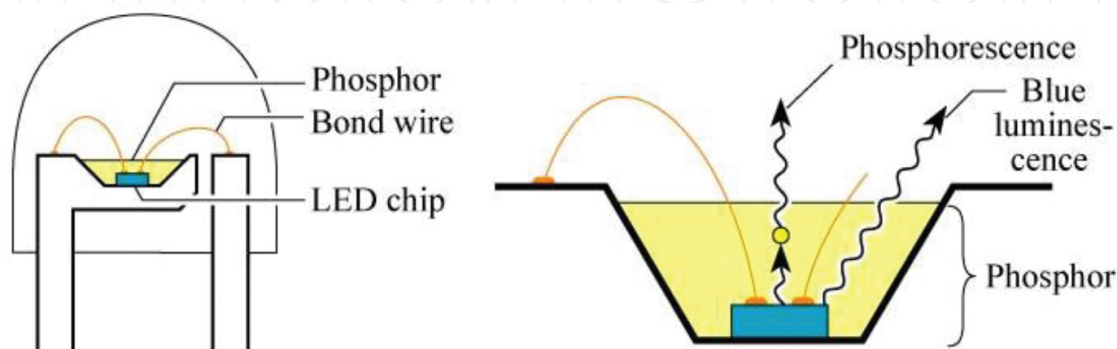


Figure 18. Schematic of phosphor converted white LED [38].

was later achieved by converting the blue LED to white LED by coupling the diode with a yellow light-emitting phosphor (**Figure 18** [38]), $Y_3Al_5O_{12}:Ce^{3+}$ [39].

7.5. Television display

One of the important applications of phosphors is in the display technology. We rely on television to watch live news and events, in full color. We use mobile phones to capture moments in color and for live video calling. All these are made possible by phosphors for display [40]. There are several technologies that are used to achieve different types of television displays, ranging from cathode ray tubes [41], liquid crystal display [42], field emission display [43], to plasma display panels [44], to mention a few. For an example, the plasma display panels (**Figure 19**) [45] have pixels that consist of small gas-discharge cells [37]. The gas is made of Xe-Ne plasma, which excites the phosphor with a vacuum ultra-violet source of 147 and 172 nm [44, 46].

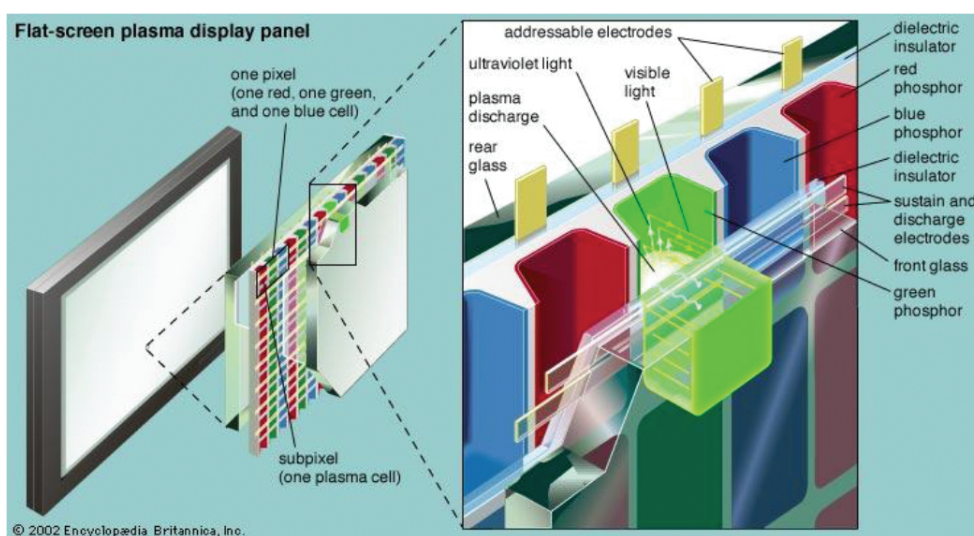


Figure 19. A schematic showing pixels of a plasma display panel [45].

8. Conclusions

The concept of luminescence, though not fully understood in the light of persistent luminescence, it has advanced the human life. The mentioned applications are of great significance in the way we live today and are only a handful of the broader applications in the technological applications. Some of which are not listed. The luminescence expected to contribute vastly in different fields, such as home lighting using electricity free light bulbs and in improving the efficiency of the solar cells.

Acknowledgements

We sincerely appreciate the funding from the South African National Research Foundation and the Erasmus Mundus EU-SATURN. Many thanks to Raphael Nyenge, who allowed me to do experiments on his sample, and the Lumilab in Belgium for opening doors for me to carry out research work. We extend gratitude to the University of the Free State, where most of the experiments were performed.

Author details

Luyanda L. Noto¹, Hendrik C. Swart², Bakang M. Mothudi¹, Pontsho S. Mbule¹ and Mokhotjwa S. Dhlamini^{1*}

*Address all correspondence to: dhlamms@unisa.ac.za

1 Department of Physics, University of South Africa, Pretoria, South Africa

2 Department of Physics, University of the Free State, Bloemfontein, South Africa

References

- [1] D.D. Busch, Nikon D200 Digital Field Guide, 2006, Wiley Publishers, Indianapolis, IN.
- [2] L.L. Noto, M.Sc. Thesis, 2011, University of the Free State, South Africa.
- [3] F. Stavale, N. Nilius, H.J. Freund, J. Phys. Chem. Lett. 4 (2013) 3972.
- [4] I. Pelant, J. Valenta, Luminescence Spectroscopy of Semiconductor, 2012, Oxford University Press, Oxford, UK.
- [5] R.C. Ropp, Luminescence and the Solid State, 2012, Elsevier Science Publishers B.V., Amsterdam, Netherlands.
- [6] J. Breithaupt, New Understanding Physics for Advanced Level, 2000, 4th ed., Nelson Thornes Ltd., London, UK.
- [7] C.T. Sah, Fundamentals of Solid-state Electronics: Solution Manual, 1996, World Scientific Publishing Co. Pte Ltd., London.
- [8] L.L. Noto, M.L. Chithambo, O.M. Ntwaeaborwa, H.C. Swart, Powder Technol. 247 (2013) 147.
- [9] J.R. Lakowicz, Principles of Fluorescence Spectroscopy, 2006, 3rd ed., Springer Publishers, New York, NY.

- [10] J. Holsa, The Electrochemical Society Interface meeting, Winter 2009, http://www.electrochem.org/dl/interface/wtr/wtr09/wtr09_p042-045.pdf [09 March 2016].
- [11] T.G. Chasteen, S. Houston, Relaxation mechanism for excited state molecules http://www.shsu.edu/chm_tgc/chemilumdir/JABLONSKI.html [09 March 2016].
- [12] A.J. Pesce, C. Rosen, T.L. Pasby, Fluorescence Spectroscopy—an Introduction for Biology and Medicine, 1971, Marcel Dekker Inc, New York, NY, p 34.
- [13] P.W. Hawkes, Advances in Electronics and Electron Physics, 1990, vol. 79, Academic Press Inc, Cambridge, UK, p285.
- [14] L.L. Noto, S.S. Pitale, M.A. Gusowki, O.M. Ntwaeaborwa, J.J. Terblans, H.C. Swart, J. Lumin. 145 (2014) 907.
- [15] P.T. Diallo, P. Boutinaud, R. Mahiou, J.C. Cousseins, Phys. Stat. Sol. (a) 160 (1997), 255.
- [16] B.J. Nyman, M.E. Bjorketun, G. Wahnstrom, J. Sol. Stat. Ionics. 189 (2011), 19.
- [17] P.J. Deren, R. Pazik, W. Streck, P. Bautinaud, R. Mahiou, J. Alloy Compd. 451 (2008), 595.
- [18] E.J. Popovici, M. Nazarov, L. Muresan, D.Y. Noh, E. Bica, M. Morar, I. Arellano, E. Indrea, Phys. Proc. 2 (2009), 185.
- [19] L.L. Noto, PhD Thesis, 2014, University of the Free State, South Africa.
- [20] V. Pagonis, G. Kitis, C. Furetta, Numerical and Practical Exercises in Thermoluminescence, 2006, Springer and Business Media Inc., New York, NY.
- [21] L.L. Noto, O.M. Ntwaeaborwa, M.Y.A. Yagoub, H.C. Swart, Mater. Res. Bull. 70 (2015) 545.
- [22] C. Furetta, Handbook of Thermoluminescence, 2003, World Scientific Publishing, Singapore.
- [23] S.W.S McKeever, Thermoluminescence of Solids, 1985, Cambridge University Press, New York, NY.
- [24] K.S. Chung, H.S. Choe, J.I. Lee, J.L. Kim, S.Y. Chang, Radiat. Prot. Dosim. 115 (2005) 1.
- [25] M.S. Dhlamini, PhD Thesis, 2008, University of the Free State, South Africa.
- [26] J. Chen, J.X. Zhao, Sensors 12 (2012) 2414. <http://krauthammerlab.med.yale.edu/imagefinder/ImageDownloadService.svc?articleid=3438444&file=fendo-03-00100-g001&size=SMALL> [18 May 2016].
- [27] F. Artizzu, F. Quochi, L. Marchiò, E. Sessini, M. Saba, A. Serpe, A. Mura, M.L. Mercuri, G. Bongiovanni, P. Deplano, J. Chem. Lett. 4 (2013) 3062.
- [28] A. Pandey, V. K. Rai, V. Kumar, V. Kumar, H. C. Swart, Sens. Actuators B, 209 (2015) 352.
- [29] P. Anurag, C. Hendrik. Swart, J. Lumin., 169 (2016) 93.

- [30] R.L. Nyenge, PhD thesis, 2015, University of the Free State, South Africa.
- [31] H.C. Swart, J.S. Sebastian, T.A. Trottier, S.L. Jones, P.H. Holloway, *J. Vac. Sci. Technol.* 14(3) (1996) 1697.
- [32] P. Boutinaud, R. Mahiou, E. Cavalli, M. Bettinelli, *Chem. Phys. Lett.* 418 (2006) 185.
- [33] <http://blocksandbricks.co.za/blocks-and-bricks/meet-the-glow-in-the-dark-brick/> [28 April 2014].
- [34] T. Maldiney, A. Bessiere, J. Seguin, E. Teston, S.K. Sharma, B. Viana, A.J.J. Bos, P. Dorenbos, M. Bessodes, D. Gourier, D. Scherman, C. Richard, *Nat. Mater.* 13 (2014) 418.
- [35] V. K. Rai, *Appl. Phys. B*, 88 (2007) 297–303.
- [36] Y. Shen, X. Wang, H. He, Y. Lin, C.-W. Nan, *Compos. Sci. Technol.*, 72 (2012) 1008–1011.
- [37] S.F. Leon-Luis, U.R. Rodriguez-Mendoza, E. Lalla, V. Lavin, *Sens. Actuators B*, 158 (2011) 208.
- [38] S. A. Wade, S. F. Collins, G. W. Baxter, *J. Appl. Phys.*, 94 (2003) 4743.
- [39] S. K. Singh, K. Kumar, S. B. Rai, *Sens. Actuators A*, 149 (2009) 16.
- [40] V. K. Rai, A. Pandey, R. Dey, *J. Appl. Phys.*, 113 (2013) 083104.
- [41] Anurag Pandey, Vineet Kumar Rai, Vijay Kumar, Vinod Kumar, H. C. Swart, *Sens. Actuators B: Chem.*, 209 (2015) 352–358.
- [42] Z.J. Li, Y.J. Zhang, H.W. Zhang, H.X. Fu, *J. Micro. Meso. Mater.*, 176 (2013) 48.
- [43] NobelPrize, http://www.nobelprize.org/nobel_prizes/physics/laureates/2014/press.html (20 March 2016).
- [44] <https://www.ecse.rpi.edu/~schubert/Light-Emitting-Diodes-dot-org/chap21/F21-07%20Nichia%20wh%20LED%20structu.jpg> (20 March 2016).
- [45] X. Zhang, W. Liu, G.Z. Wei, D. Banerjee, Z. Hu, J. Li, *J. Am. Chem. Soc.*, 136 (40) (2014) 14230.
- [46] W.M. Yen, S. Shionoya, H. Yamamoto, *Phosphor Hand Book*, 2nd ed., 2007, CRC Press, Boca Raton, FL.